Journal of Sound and Vibration (1999) **221**(4), 607–621
Article No. jsvi.1998.2042, available online at http://www.idealibrary.com on IDEAL

DYNAMICS AND ROBUST CONTROL OF A HIGH SPEED OPTICAL PICKUP

S. LIM AND T.-Y. JUNG
Department of Mechanical Engineering, MyongJi University, Yongin, Korea

(*Received* 16 *February* 1998, *and in final form* 19 *October* 1998)

Recently there has been an increasing demand for optical disk drives to have higher speed as well as high information density, especially for applications like CD-ROM drives. To this end improvement of their optical pickup structure and control is recognized as a very challenging issue. In this paper, the pickup is first analytically modelled in a plane to describe its coupled auto-focusing and auto-tracking systems. With its immeasurable parameters being estimated based on experimental data, an approximate 1-DOF linear model is obtained neglecting the coupling terms. To design the high speed and robust positional servo controller realistic design specifications are addressed, and the H_∞ control method is employed. Finally taking as an example the pickup in a commercial CD-ROM drive, the performance of the designed controller is verified through realtime experiments.

1. INTRODUCTION

Recently optical disk drives are being widely used as computer CD-ROM drives as well as CDP, LDP, DVD, etc. However, CD-ROM drives currently available are still not fast enough compared to the competing hard disk drives so that further design innovations are in need. Aside from the structural point of view [1, 2], this paper is intended to aid such a trend by proposing a model describing key dynamics of the optical pickup, which is the major component of optical disk drives, and its robust servo controller.

In Figure 1, a very popular linear-tracking, wire-supported type optical pickup in a commercial 8 fold speed CD-ROM drive is illustrated. Among a total of five servo systems involved [3], two possess the most unique features and are regarded as very challenging techniques for increasing its data access speed. One is the auto-focusing (AF) servo, which keeps the waist of the laser beam passing through the objective lens always on the disk pit's reflection surface. The other is the auto-tracking (AT) servo to radially position the focus finely onto the spiral track following the action of a coarse tracking motor. Those two servos are desired to independently function in mutually orthogonal directions despite the ordinary deficiencies and vibrations of the disk while it rotates with a constant linear velocity [3].

0022–460X/99/040607 + 15 $30.00/0

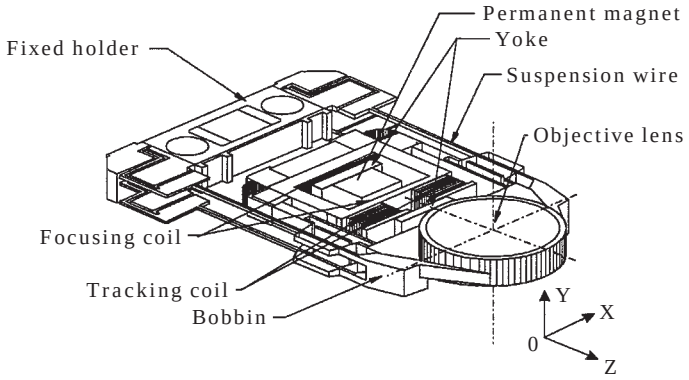

Figure 1. Schematic diagram of a pickup.

Even if some researchs have been done exclusively on the AT servo [4, 5], AF and AT servos are basically problems of the same nature in that they are both position control systems of a flexible supporter's tip using the voice coil type actuators. Hence, this paper mainly deals with the AF servo system.

2. SYSTEM EQUATION

The AF control system generally consists of a feedback controller, a power amp., a pickup structure, and a position error sensor, as in Figure 2. Among such components, the equations of motion for the pickup are first to be derived and others will be treated subsequently to form the overall system equation.

2.1. EQUATIONS OF PICKUP MOTION

The way of supporting the bobbin varies with manufacturers, but basically the bobbin is made to translate in parallel with the fixed holder. It is due to the parallelepiped structure composed of flexible supporting elements with some viscoelastic materials glued on to increase motional damping. Hence, taking the

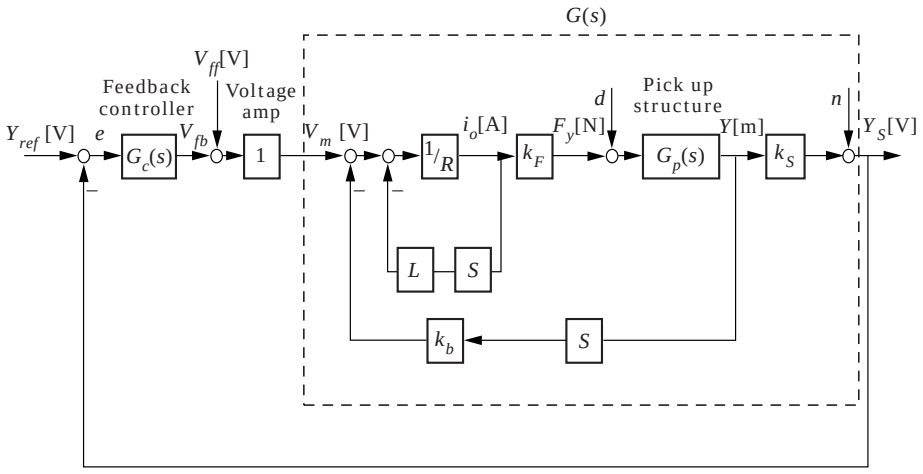

Figure 2. Block diagram of the AF servo system.

pickup in Figure 1 as a typical one, its equations of motion are to be derived. In general, vibration of the pickup can be simply modelled as a lumped mass–spring–damper system in the operating frequency range due to the rigidity of bobbin material and the high mass ratio of bobbin to suspension wires [6]. That is, higher bending modes of suspension wires can be neglected.

However, in the process of pickup assembly, it is almost impossible to exactly match the mass center with the centroid where the resultant actuator forces are acting. This causes some undesirable dynamics coupling the AF and AT motions by way of the torsional mode of the bobbin. In spite of the damping treatment, such a coupling mode is hard to remove completely. On the other hand, the remaining 3 motional DOF's of the bobbin in space are relatively hard to obtain due to the parallelepiped suspension mechanism, which means that their natural frequencies exist far beyond the operating frequency range [1, 2].

Therefore, in this section, it will be analytically investigated how the torsioal motion occurs through a planar model of the pickup. In Figure 3, the bobbin is assumed rigid. Therefore it can translate along the X and Y axes, and rotate about the Z axis, being restrained by massless springs. And, the electromagnetic actuator forces from the actuators are assumed to be uniformly distributed over the bobbin and acting along the body-fixed co-ordinate frame xyz.

Here, it is taken into account that the mass center does not coincide with the centroid. To derive equations of motion, the displacement vector $\mathbf{w}$ of a typical point on the bobbin is first found with respect to the origin of the inertial XYZ co-ordinate frame.

$$\mathbf{w} = \mathbf{R} + {}^0C_1\mathbf{r} \tag{1}$$

where $\mathbf{R} = [X \;\; Y]^T$ is the position vector of the centroid form the origin O,

$${}^0C_1 = \begin{bmatrix} c\theta & -s\theta \\ s\theta & c\theta \end{bmatrix}$$

is the rotation matrix between the two frames, $\mathbf{r} = [x \;\; y]^T$ is the position vector of the typical point from the centroid o, and $c\theta$ and $s\theta$ are abbreviations of cos θ and sin θ, respectively.

Considering the time derivative of equation (1), one can get the kinetic energy expression as follows:

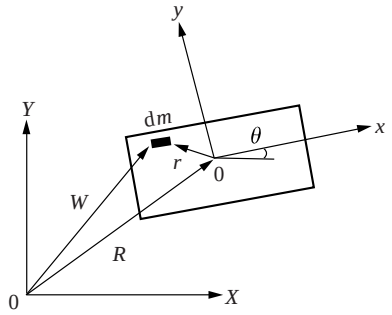

Figure 3. Planar model.

$$T = \frac{1}{2}\int_m \dot{\mathbf{w}}^T\dot{\mathbf{w}}\,\mathrm{d}m$$
$$= \frac{1}{2}m(\dot{X}^2 + \dot{Y}^2) + \frac{1}{2}I_{oz}\dot{\theta}^2 - \dot{X}\dot{\theta}(S_x s\theta + S_y c\theta) + \dot{Y}\dot{\theta}(S_x c\theta - S_x s\theta), \qquad (2)$$

where I_{oz} is the mass moment of inertia of the bobbin about its centroid while $S_x = \int_m x\,\mathrm{d}m$ and $S_y = \int_m y\,\mathrm{d}m$ are first mass moments of inertia. Here, it is noteworthy that those first mass moments of inertia do not vanish as long as the centroid is not coincident with its mass center. Next, the potential energy is derived as

$$V = \frac{1}{2}(k_x X^2 + k_y Y^2 + k_\theta \theta^2) + mgY, \qquad (3)$$

where k_x, k_y, and k_θ denote spring stiffness in each direction, and g the gravitational acceleration. The non-conservative virtual work is obtained as in equation (4)

$$\delta\bar{W} = \int_A ({}^0C_1\mathbf{f})^T\delta\mathbf{w}\,\mathrm{d}A$$
$$= (F_x c\theta - F_y s\theta)\delta X + (F_x s\theta + F_y c\theta)\delta Y, \qquad (4)$$

where F_x and F_y represent the actuator forces resulting at the centroid respectively in the AT and AF directions. Note that no provisions are yet made for actuating the torsional motion in the contemporary optical pickups.

Plugging equations (2) through (4) into the standard Lagrangian equation [7], the equations of bobbin motion can be readily obtained:

$$M\ddot{\mathbf{q}} + K\mathbf{q} + \mathbf{b} + \mathbf{g} = \mathbf{f}, \qquad (5)$$

where $\mathbf{q} = [X\ \ Y\ \ \theta]^T$ is the generalized co-ordinate, M and K are overall mass and stiffness matrices, $\mathbf{b}$ is the centrifugal and Coriolis force term, and $\mathbf{f}$ is the actuator force vector. Their detailed expressions are as follows:

$$M = \begin{bmatrix} m & 0 & -(S_x s\theta + S_y c\theta) \\ 0 & m & (S_x c\theta - S_y s\theta) \\ -(S_x s\theta + S_y c\theta) & (S_x c\theta - S_y s\theta) & I_{oz} \end{bmatrix},$$
$$K = \mathrm{diag}[k_x, k_y, k_\theta], \quad f = [F_x c\theta - F_y s\theta,\ F_x s\theta + F_y c\theta,\ 0]^T,$$
$$\mathbf{b} = -\begin{bmatrix} \dot{\theta}^2(S_x c\theta - S_y s\theta) \\ \dot{\theta}^2(S_x s\theta + S_y c\theta) \\ \dot{X}\dot{\theta}(S_x c\theta - S_y s\theta) - \dot{Y}\dot{\theta}(S_x s\theta + S_x c\theta) \end{bmatrix}, \quad \mathbf{g} = \begin{bmatrix} 0 \\ mg \\ 0 \end{bmatrix}.$$

In the stiffness matrix above k_θ is in fact related to the other elements such that

$$k_\theta = \frac{B^2 + H^2}{16\sqrt{c^2\alpha/k_x^2 + s^2\alpha/k_y^2}}, \tag{6}$$

where the angle, α, equals $\pi/2 - \tan^{-1}(H/B)$, and B and H are respectively the horizontal and vertical gaps between the suspension points. Therefore, to make the torsional stiffness increase, it is recommended that there be as wide a spacing between suspensions as possible.

2.2. LINEARIZED OVERALL SYSTEM EQUATION

To design a linear controller and identify system parameters based on the frequency response functions (FRF), the equations of motion need to be linearized. That is, assuming θ to be small and neglecting second and higher order perturbation terms, equation (5) can be recast as

$$M_l\ddot{\mathbf{q}} + C\dot{\mathbf{q}} + K\mathbf{q} + \mathbf{g} = \mathbf{f}_l, \tag{7}$$

where the damping term is addtionally introduced to reflect the effect of the viscoelastic materials, and the centrifugal and Coriolis terms have disappeared with the following new coefficients being

$$M_l = \begin{bmatrix} m & 0 & -S_y \\ 0 & m & S_x \\ -S_y & S_x & I_{oz} \end{bmatrix}, \quad C = \begin{bmatrix} c_x & 0 & 0 \\ 0 & c_y & 0 \\ 0 & 0 & c_\theta \end{bmatrix}, \quad \mathbf{f}_l = [F_x \quad F_y \quad 0]^T.$$

From equation (7), it seems clear that the non-zero S_x and S_y quantities play the role of coupling AF and AT motions. Hence, to reduce the undesirable AT motion caused by AF servo, at least one of them has to be tailored to be as small as possible unless some provision is made for actively suppressing the torsional mode.

Now, an expression for the transfer function $G(s)$ needs seeking from the controller output V_{fb} to the measured bobbin displacement Y_s in Figure 2, since extra devices such as a power amplifier, an actuator, and a displacement sensor are always involved. In this paper, a voltage type power amplifier with unity gain is used, as shown in Figure 4. Thus the output current i_o is not proportional to the input voltage V_m. Instead, due to the back EMF (electromotive force) generated by the motion of the suspension wires serving also as electric conduits across the magnetic flux, equation (8) holds from Kirchhoff's voltage law.

$$V_m - i_o R - L\frac{\mathrm{d}i_o}{\mathrm{d}t} - k_b\dot{Y} = 0, \tag{8}$$

where R, L, and k_b represent the voice coil's resistance, inductance, and back EMF constant, respectively.

Defining the force constant k_F and the sensor gain k_s, one can get the desired AF transfer function as in the Appendix from equations (7) and (8). Likewise, the AT transfer function can be obtained with the exception of negligible back EMF constant.

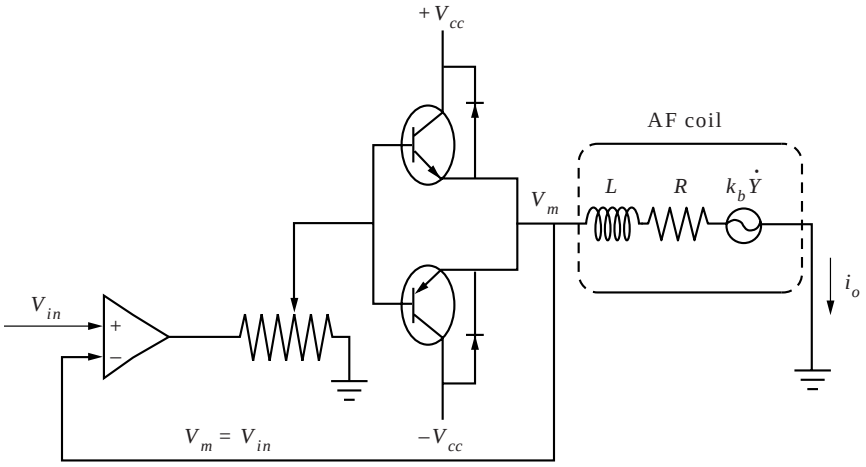

Figure 4. Power amplifier.

2.3. SYSTEM PARAMETER IDENTIFICATION

Given the experimental FRF in the AF or AT direction, it is feasible to estimate the immeasurable system parameters like k_x, k_y, k_b, etc. Among numerous methods, the least square error curve fit method is adopted here. That is, unknown parameters are to be estimated so as to minimize a certain performance index

$$J = |||G(j\omega)| - |\hat{G}(j\omega)|||^2 = \sum_i (|G(j\omega_i)| - |\hat{G}(j\omega_i)|)^2, \quad i = 1, 2, \ldots, \qquad (9)$$

in which $\|.\|$ denotes the Euclidean vector norm, and $\hat{G}(j\omega)$ the estimate of $G(j\omega)$. As long as the number of data, i, is large enough compared to that of unknowns, such a non-linear optimization problem can be efficiently solved by the Levenberg–Marquardt method [8] with a reasonable initial guess of unknown parameters.

3. H_∞ FEEDBACK CONTROLLER DESIGN

Prior to controller design the required performance and stability goals have to be specified in consideration of actual operating circumstance. For instance, in the case of the AF system the disk vibration in the Y direction corresponds to the reference input whereas the vibration of the CD-ROM drive base is transmitted as the disturbance force d in Figure 2. Such a disturbance can be readily found, $c\dot{Y}_e + kY_e$ referring to Figure 5, where Y_e represents the oscillatory displacement of the base. Its effect on the control performance needs to be investigated.

On the other hand, for the controller design the linearized mathematical model derived above is to be used with its coupling term neglected. Therefore, it will always contain model uncertainties to some degree in addition to those arising from neglected non-linearities in the high frequency range, parameter

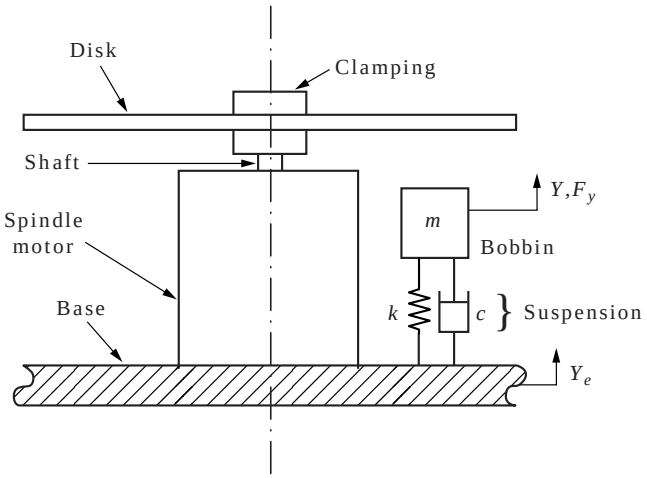

Figure 5. External disturbance.

variations, etc. This should be taken into account for stability specification. Furthermore, robust performance and stability should be secured within the available power supply from computers, which means in turn that a control input higher than a few volts in either direction could be fatal to the life of voice coils.

For performance specification magnitude of the sensitivity [9], S equal to $e(s)/Y_{ref}(s)$, should be predetermined in the frequency domain. Among others, the disk vibration is mainly caused by its surface deficiency even though it is being regulated not to exceed a certain level by ISO [10]. For instance, the FRF's of disk vibration at inner tracks are experimentally obtained to be presented in Figure 6. In general, as in a 2nd order vibrational system the vibration magnitude keeps increasing up to the resonance frequency coincident with the spindle speed, and afterwards decreases with a constant acceleration. And, the peak magnitude tends to decrease with the spindle speed due to the larger stiffening centrifugal force, which will look more evident in Figure 11 than here.

Hence, given the desired maximum spindle speed for a CD-ROM drive, a curve seems acceptable as the reference input magnitude, which constantly has the peak magnitude below the resonance frequency and a constant slope of -40 dB/Dec, above it. However, some extra DC gain is necessary to attenuate the effects of low frequency disturbances such as the base vibration, the inclination of the turn table, and so on. On the other hand, the required positional accuracy in the AF direction is smaller than ± 1 μm. Thus, from the following equation one can get the conditions to meet the desired performance in terms of the loop transfer function, $L(s)$, in the low frequency range;

$$|S(\omega)| = \left|\frac{1}{1 + L(\omega)}\right| \cong |L(\omega)^{-1}|. \tag{10}$$

Moreover, the cut-off frequency ω_c should be as high as possible for fast speed. However, taking into account the destabilizing effect of unmodelled high frequency vibrational modes and an excessive power demand during the

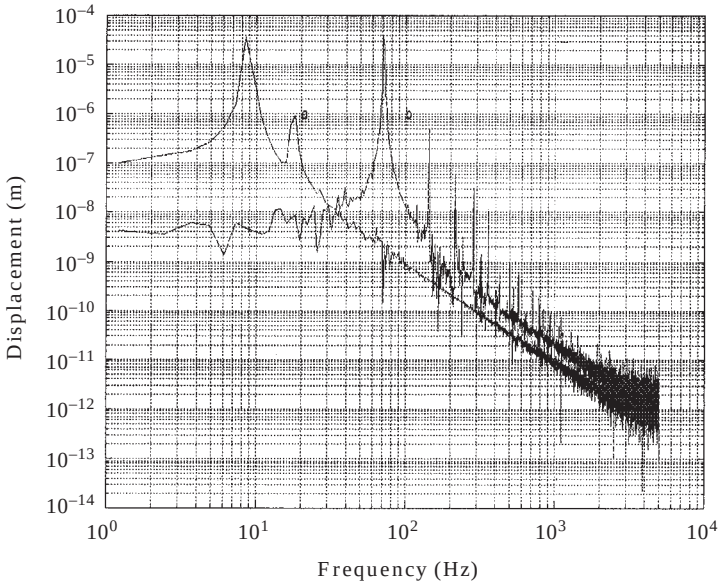

Figure 6. Disk vibrations: (a) $1\times$, (b) $8\times$.

transient state, some trade-off is inevitable. Thus, it is recommended that ω_c be decided for the open loop system to cover only up to the frequency where the so-called reference input magnitude of disk vibration equals the required positional accuracy.

For securing the stability in the presence of unmodelled dynamics, the roll-off rate of $L(s)$ should be limited to -20 dB/Dec, in the ω_c neighborhood, and afterwards steeper than it. Due to the small magnitude of $L(s)$ in the high frequency range, equation (11) holds for the complementary sensitivity:

$$T(s) = \frac{L(s)}{1 + L(s)} \cong L(s). \tag{11}$$

On the other hand, some means is also necessary to counteract the bobbin deflection caused by its weight. Otherwise the focus error signal itself could not be obtained whatsoever in actual CD-ROM drives, and the feedback control voltage V_{fb} could be too high in the transient state due to the large control gain. This can be handled by feeding forward an additional constant input

$$V_{ff} = Ri_o = R\frac{mg}{k_F}. \tag{12}$$

To meet the aforementioned specifications, various control design methods can be considered. However, since disk drives use the laser sensor only to measure the gap in between the pit and the objective lens for the AF servo, many candidates are eliminated including a series of modern control methods which estimate state variables from the system outputs other than errors. This is a good reason for using the conventional PID control with phase compensations

in this application. However, the loop shaping process by finding its suitable associated parameters is indeed a time-consuming iterative job.

Hence, to avoid such an inefficiency the H_∞ control method [11] is applied which guarantees the robustness with the advantage of a fully mechanized design process. In order to get the H_∞ controller satisfying the design specifications, the minimization problem of a mixed sensitivity is proposed as

$$\left\| \begin{bmatrix} W_1 S \\ W_3 T \end{bmatrix} \right\|_\infty < 1, \tag{13}$$

where $\|.\|_\infty$ means the H_∞ norm, and W_1 and W_3 denote weight functions to be defined in the frequency domain consistently with the aforementioned desired loop shape of $L(s)$. Note here that if equation (13) is optimally solved, W_1 will approximate $L(s)$ below the cut-off frequency whereas W_3^{-1} will approximate $L(s)$ above it. Given equations (13) and the weight functions, the H_∞ feedback controller can be synthesized by simply following the procedure in reference [11].

4. NUMERICAL SIMULATION AND EXPERIMENTS

All the contents addressed hereto are applied to the pickup in Figure 1.

4.1. PARAMETER IDENTIFICATION

Using a dynamic signal analyzer and a laser Doppler vibrometer, FRF's in both AF and AT directions are obtained as in Figure 7. In so doing, an impulse signal was input from the PC and the output signals were sampled at the period of 0·1 ms. Even though there remain some noisy signals, the FRF's show the three vibrational modes mentioned in section 2 clearly in the concerned frequency range. In fact, the next vibrational mode was found around 5 kHz. Compared to the AF direction the pickup has higher stiffness in the AT direction. As a result, in the AT direction the DC gain is smaller, and the resonance frequency is higher so that the cross-coupling torsional mode is almost invisible.

After all the measurable parameters are found as in Table 1, the other system parameters can be estimated according to equation (9) based on the data in Figure 7. Here the lumped mass–spring–damper model is used for pickup dynamics neglecting the cross-coupling, since such a simple model is to be adopted for the controller synthesis. Making use of the first 100 data points of each FRF curve, final estimates are obtained as in Table 2.

Accordingly, it can be deduced from the mass and natural frequencies that $\hat{k}_x = 30{\cdot}9511$ N/m and $\hat{k}_y = 13{\cdot}2264$ N/m. Moreover the damping coefficient in each direction can be computed from the relation $c = 2\zeta\sqrt{mk}$. In this case the simple model takes the FRF in Figure 7(b) with some estimation errors.

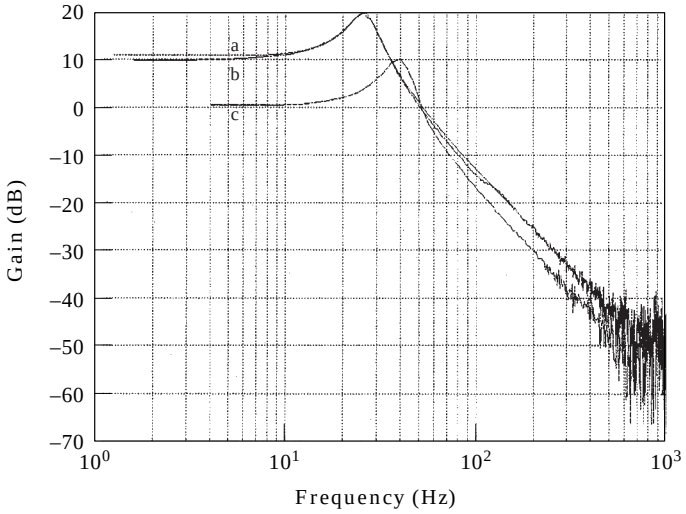

Figure 7. FRF's: (a) AF, (b) AF estimate, (c) AT.

4.2. CONTROLLED PERFORMANCE

The weight functions are defined as

$$W_1 = 10^3\left(\frac{s}{\omega_2}+1\right)^2 \Big/ \left(\frac{s}{\omega_1}+1\right)^3, \quad \text{and} \quad W_3 = 10^5 s^3/\omega_3^3$$

as plotted in Figure 8 where the relevant corner frequencies ω_1, ω_2, and ω_3 are set respectively at 5×10^2, 3×10^3, and 10^6 rad/s. The following are taken into account: the maximum spindle speed amounts to about 70 Hz, the peak vibrational magnitude about 100 μm, the extra DC control gain about 20 dB, the corner frequency about 3·2 kHz, and the roll-off rate in high frequency range −60 dB/Dec.

With such weight functions the transfer function of the designed H_∞ feedback controller turns out to be

$$G_c(s) = \frac{\begin{array}{r}3257s^5 + 1{\cdot}839\times10^8 s^4 + 7{\cdot}637\times10^{11}s^3 + 1{\cdot}041\\ \times10^{15}s^2 + 7{\cdot}301\times10^{16}s + 2{\cdot}691\times10^{19}\end{array}}{\begin{array}{r}s^5 + 4{\cdot}813\times10^4 s^4 + 1{\cdot}156\times10^9 s^3 + 1{\cdot}666\\ \times10^{12}s^2 + 8{\cdot}314\times10^{14}s + 1{\cdot}51\times10^{17}\end{array}}.$$

TABLE 1

Measured system parameters

	AF direction	AT direction
R (Ω)	7·5	7·28
k_s (V/μm)	1/320	1/320
L (mH)	0·144	0·0223
m (kg)	0·49e-3	0·49e-3

TABLE 2
Estimated system parameters

	AF direction	AT direction	Remark
$\widehat{k_b}$ (V/(m/s))	0·1066569	Negligible	
$\hat{\zeta}$	0·1520755	0·1520755	Damping factor
$\widehat{\omega_n}$ (rad/s)	164·2944561	251·3274123	Natural frequency
$\widehat{k_F}$ (N/A)	0·09837956	7·210e-2	

In such a case the open loop transfer function appears as in Figure 9, where the gain and phase margins are observed to be respectively 9·923 dB and 43·81° and the bandwidth about 2×10^4 rad/s. Such an analog controller is reduced by one order using the balanced realization method [12] and cast into a discrete time controller by the bilinear transform [13] with the sampling frequency of 32 kHz.

To see how the digital controller performs in practice, an experimental set-up is built as in Figure 10. The vibrometer and the numerical integrator take the place of the built-in focus error sensor, whereas the stored reference signal does the vibration of the spinning optical disk.

With the initial conditions assumed to be zero, the AF system is servoed to yield such results as in Figure 11, where the top four curves show the case of $1\times$ speed and the other four curves the case of $8\times$ speed. In so doing the number of the original disk vibrational data has been increased by a linear interpolation to match the sampling period of the discrete realtime control. In Figure 11 the control performance proves good enough in terms of speed and accuracy within the admissible range of control input voltage. This also implies the robustness of the controller in that the experimental results satisfy the design specifications even if the simple model contains some uncertainties. In fact, the controller was also experimentally confirmed to work even in the case of a $16\times$ speed CD-

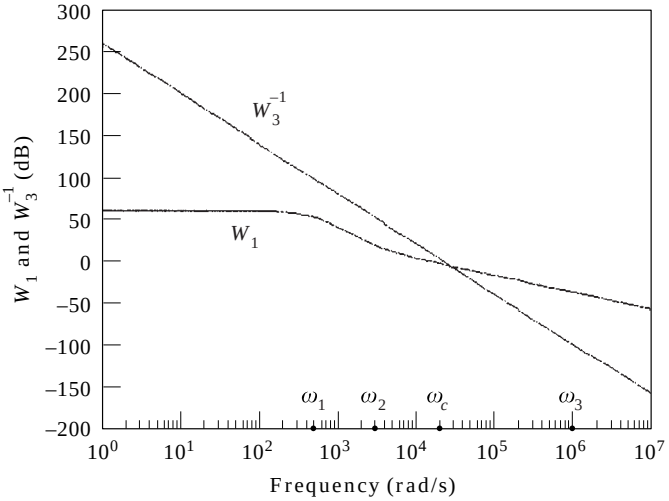

Figure 8. Weight functions.

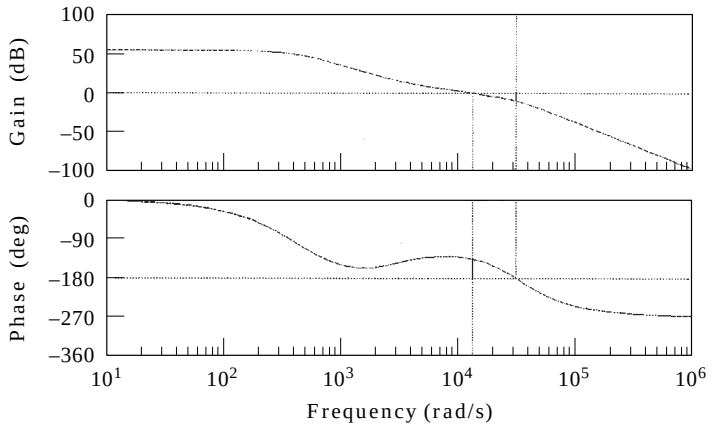

Figure 9. Loop transfer function.

ROM drive assuming slightly smaller disk vibration than that of an $8\times$ speed one.

In addition, the disturbance effect can be evaluated by observing the magnitude of the transfer function from Y_e to Y in Figure 2. Referring to Figure 12, the effect is seen to be well suppressed by the designed feedback controller over a wide frequency range. On the other hand, numerical simulations indicate that the displacement in the AT direction caused by the AF servo system oscillates within about $\pm 0{\cdot}1$ μm in case the eccentricity of 0·12 and 0·01 mm exists in the x and y directions, respectively.

5. CONCLUSIONS

An optical pickup is modelled analytically in a plane to describe its coupled AF and AT motions, and subsequently linearized combining actuator dynamics. With its immeasurable system parameters estimated based on experimental data,

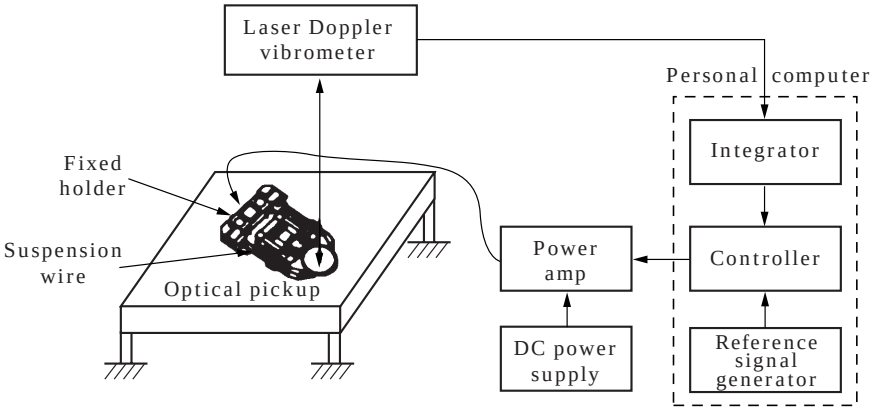

Figure 10. Experimental set-up.

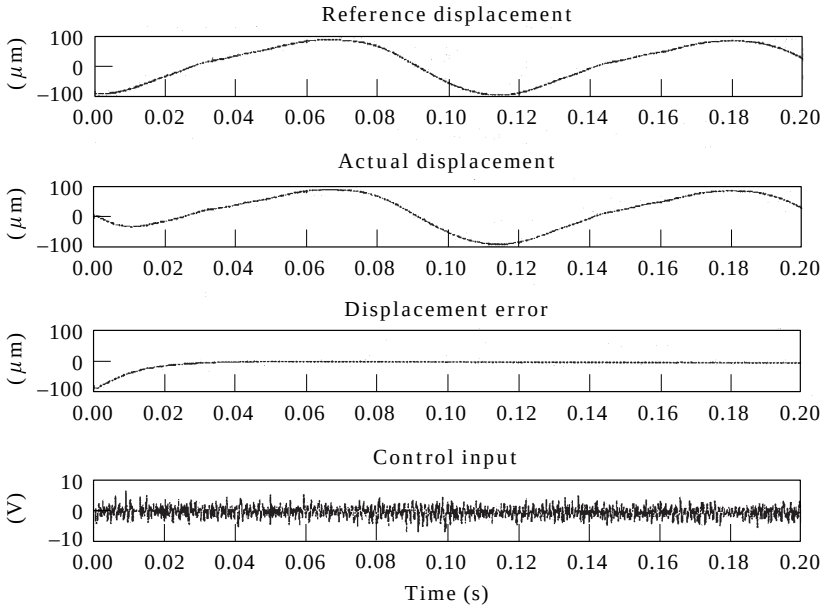

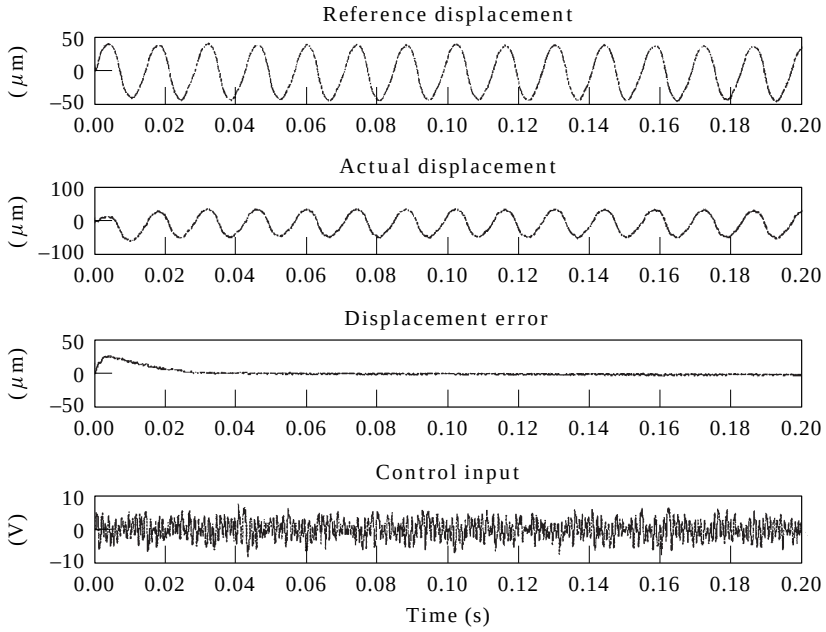

Figure 11. AF controlled performance.

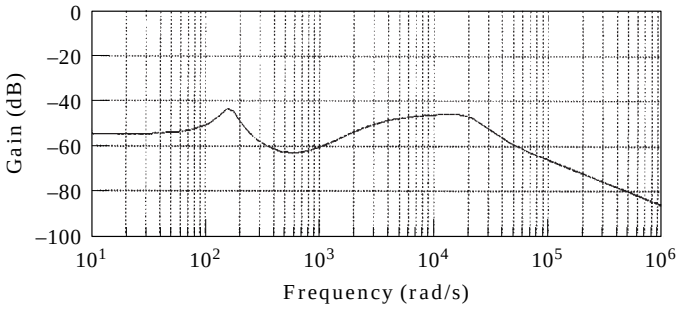

Figure 12. Disturbance effect.

such a model enables one to predict the interference between the AF and AT servo systems and can be used in a decoupled form for designing the AF positional servo controller. The desired servo performance and stability are specified in terms of the loop transfer function in the frequency domain. To achieve loop shaping the H_∞ control scheme turns out to be appropriate and efficient.

An experimental set-up is built involving the pickup in a commercial high speed CD-ROM drive. A series of experiments prove the good performance and stability robustness of the designed feedback controller under some realistic power limitations.

Finally it may be worthwhile to mention three ways to further increase the speed of the AF or AT servo system more than ever with the present pickup structure retained. The first is reducing the pickup weight further down. Second is increasing the available power supply. The last is to apply a MIMO control scheme employing extra light actuators to suppress the undesirable coupling modes in the high frequency range.

REFERENCES

1. I. KAJIWARA and A. NAGAMATSU 1993 *Journal of Vibration and Acoustics* **115**, 377–383. Optimum design of optical pick-up by elimination of resonance peaks.
2. K. LIM, Y. LEE, S. KIM and J. LEE 1995 *Proceedings of the Korean Society for Noise and Vibration Engineering*, 258–263. Dynamic characteristics of actuator for high density optical recording pick-up (in Korean).
3. K. C. POHLMANN 1992 *The Compact Disc Handbook*. Oxford: Oxford University Press.
4. W. DRAIJER, M. STEINBUCH and O. H. BOSGRA 1992 *Automatica* **28**, 455–462. Adaptive control of the radial servo system of a compact disc player.
5. H. G. M. DOTSCH, H. T. SMAKMAN, P. M. J. VAN DEN HOF and M. STEINBUCH 1995 *Proceedings of IEEE Conference on Decision and Control*, 1720–1725. Adaptive repetitive control of a compact disc mechanism.
6. S. LIM and Y. Y. KIM 1996 *Proceedings of the 4th IASTED International Conference on Robotics and Manufacturing*, 221–223. H^∞ Servo control of optical pick-ups.
7. L. MEIROVITCH 1967 *Analytical Methods in Vibrations*. London: Macmillan.
8. D. MARQUARDT 1963 *SIAM Journal of Applied Mathematics* **11**, 431–441. An algorithm for least-squares estimation of nonlinear parameters.

9. J. M. MACIEJOWSKI 1989 *Multivariable Feedback Design*. New York: Addison-Wesley.
10. *ISO/IEC* 10149 1995 *Information Technology—Data Interchange on Read-Only* 120 *mm Optical Data Disks (CD-ROM)*.
11. J. DOYLE, K. GLOVER, P. KHARGONEKAR and B. FRANCIS 1989 *IEEE Transactions on Automatic Control* **34**, 831–847. State–space solutions to standard H^2 and H^∞ control problems.
12. B. C. MOORE 1981 *IEEE Transactions on Automatic Control* **26**, 17–31. Principal component analysis in linear systems: controllability, observability, and model reduction.
13. C. L. PHILLIPS and H. T. NAGLE 1990 *Digital Control System Analysis and Design*. Englewood Cliffs, NJ: Prentice Hall; second edition.

APPENDIX: AF TRANSFER FUNCTION OF THE PICKUP

$$G(s) = \frac{N(s)}{D(s)},$$

where

$$N(s) = k_s k_F\{(mI_{oz} - S_y^2)s^4 + (mc_\theta + c_x I_{oz})s^3 + (mk_\theta + c_x c_\theta + k_x I_{oz})s^2 + (k_\theta c_x + k_x c_\theta)s + k_x k_\theta\},$$

$$\begin{aligned} D(s) =& Lm(mI_{oz} - S_y^2 - S_x^2)s^7 \\ &+ \{Rm(mI_{oz} - S_y^2 - S_x^2) + L(-c_y S_y^2 - c_x S_x^2 + mc_y I_{oz} + mc_x I_{oz} + m^2 c_\theta)\}s^6 \\ &+ \{R(-c_y S_y^2 - c_x S_x^2 + mc_y I_{oz} + mc_x I_{oz} + m^2 c_\theta) \\ &+ L(c_x c_y I_{oz} + mk_y I_{oz} + mk_x I_{oz} + m^2 k_\theta + mc_x c_\theta + mc_y c_\theta - S_y^2 k_y - k_x S_x^2) \\ &+ k_F k_b (mI_{oz} - S_y^2)\}s^5 \\ &+ \{L(c_x c_y c_\theta + mk_x c_\theta + mk_y c_\theta + k_x c_y I_{oz} + mc_x k_\theta + c_x k_y I_{oz} + mc_y k_\theta) \\ &+ R(c_x c_y I_{oz} + mk_y I_{oz} + mk_x I_{oz} + m^2 k_\theta + mc_x c_\theta + mc_y c_\theta - S_y^2 k_y - k_x S_x^2) \\ &+ k_F k_b (mc_\theta + I_{oz} S_x)\}s^4 \\ &+ \{L(k_x k_y I_{oz} + mk_x k_\theta + mk_y k_\theta + k_x c_y c_\theta + c_x c_y k_\theta + c_x k_y c_\theta) \\ &+ R(c_x c_y c_\theta + mk_x c_\theta + mk_y c_\theta + k_x c_y I_{oz} + mc_x k_\theta + c_x k_y I_{oz} + mc_y k_\theta) \\ &+ k_F k_b (mk_\theta + I_{oz} k_x + c_x c_\theta)\}s^3 \\ &+ \{R(k_x k_y I_{oz} + mk_x k_\theta + mk_y k_\theta + k_x c_y c_\theta + c_x c_y k_\theta + c_x k_y c_\theta) \\ &+ L(c_x k_y k_\theta + k_x c_y k_\theta + k_x k_y c_\theta) + k_F k_b (k_\theta c_x + k_x c_\theta)\}s^2 \\ &+ \{R(c_x k_y k_\theta + k_x c_y k_\theta + k_x k_y c_\theta) + Lk_x k_y k_\theta + k_F k_b k_x k_\theta\}s + Rk_x k_y k_\theta. \end{aligned}$$